RESPONSE OF TIDAL AND SEDIMENT DYNAMICS OF THE JIAOJIANG RIVER ESTUARY TO RECLAMATION, CHINA

Afei Hou[1] and Jianfeng Tao[2]

Utilizing flood season data from 2005 and 2014 at the Jiaojiang River estuary, we developed a three-dimensional hydrodynamic and sediment transport model. This model, integrated with mechanism decomposition of sediment flux, was employed to examine alterations in tidal and sediment dynamics, and estuarine turbidity maximum (ETM) due to reclamation. Post-reclamation observations revealed a narrowed estuary mouth, an expanded tidal range, diminished asymmetry, and intensified flooding currents. Furthermore, the suspended sediment concentration (SSC) increased by approximately 5 kg/m^3 upstream of Shixianfu (SXF) and by about 3 kg/m^3 between SXF and Haimen. The ETM shifted more than 30 km upstream, causing siltation depths to reach approximately 2 m upstream of SXF and 0.8 m between SXF and Haimen. Mechanism decomposition of sediment flux indicated that enhanced tidal pumping effects near and above SXF significantly increased sediment transport towards upstream. This primarily accounted for the increased SSC, the upstream shift, and the extended duration of the ETM.

Keywords: Jiaojiang River Estuary; Estuary Turbidity Maximum; Tidal pumping; Mechanism decomposition of sediment flux; Erosion and siltation of riverbeds

INTRODUCTION

Estuaries, influenced by both marine and terrestrial factors, are sensitive zones subject to intense human activities and global climate change. In this river section, the convergence of suspended sediments from river discharge and oceanic upwelling frequently forms a prominent estuarine turbidity maximum (called the ETM) (Glangeaud, 1938; Jay et al., 2015). Here, suspended sediment concentrations (SSC) consistently exceed those upstream and downstream, exhibiting regular fluctuations within a certain range. These hydro and sediment characteristics enrich the estuary with biological, land, harbor and navigation resources. As human societies and economies have evolved, extensive governance and development activities in many estuaries have altered their hydro and sediment dynamics and sediment transport processes (Dai et al., 2014; Sun et al., 2017; Tessler et al., 2015; Yao et al., 2023; Zhang et al., 2022). This can significantly impact the estuary, increasing the risk of developments that are detrimental to human economic interests (Wang et al., 2014).

The ETM has long been a focal point in coastal and estuarine research (e.g., Burchard et al., 2018; de Swart et al., 2009; Jay et al., 2015; Mitchell et al.,2012; Yu et al., 2014). Recently, Jay et al. (2015) and Burchard et al. (2018) have comprehensively reviewed advances in understanding the mechanisms of ETMs and sediment trapping, utilizing on-site observations, remote sensing, theoretical analyses, and numerical simulations. For specific estuary cases, Winterwerp et al. (2011) explored the causes for the transition of the Ems estuary from low to high turbidity and the upward displacement of the ETM following channel deepening. They proposed that the channel deepening intensified tidal asymmetry and modified sediment transport mechanisms. Concurrently, de Jonge et al. (2014) contended that deepening the channel in the Ems estuary elevated the water depth, diminished bottom friction, and consequently raised SSC, resulting in an upward shift of the ETM. Zhang et al. (2022) found in their analysis of the morphodynamics of the North Branch of the Yangtze Estuary that reclamation prior to 2007 intensified tidal deformation, leading to siltation in the middle and upper reaches of the channel. These all underscore the ongoing scholarly focus on the impact of human activities on estuarine dynamics, sediment transport, and geomorphology.

Located at the top of Taizhou Bay on the central coast of Zhejiang Province, China (Fig. 1a), the Jiaojiang River estuary (JRE) has a ETM extending up to 20 km (Guan et al., 1998). In recent decades, intensive human activities at the JRE have significantly altered its hydrodynamics, sediment transport, and geomorphology (Chen et al., 2008; Zhang et al., 2016; Yao et al., 2023). Since 1990, evacuating sand in channels has intensified tidal dynamics and resulted in substantial changes in riverbed erosion and deposition (Chen et al., 2008). Reclamation of JRE has also enhanced tidal dynamics (Zhang et al., 2016). Simultaneously, dredging in estuarine channels has changed sediment flux and potentially increased the thickness of the fluid mud (Yao et al., 2023). However, research on the impact of reclamation on sediment transport in the JRE remains relatively limited. Our study develops a three-dimensional hydrodynamics and sediment transport model for the JRE and Taizhou Bay, focusing on the impacts of reclamations on hydro and sediment dynamics and the distribution of the ETM from 2005 to 2014, aiming to support estuarine management and sustainable resource utilization.

[1] College of Harbor, Coastal and Offshore Engineering, Hohai Univ. Email: houafei@126.com.
[2] College of Harbor, Coastal and Offshore Engineering, Hohai Univ. Email: aoetao@hhu.edu.cn.

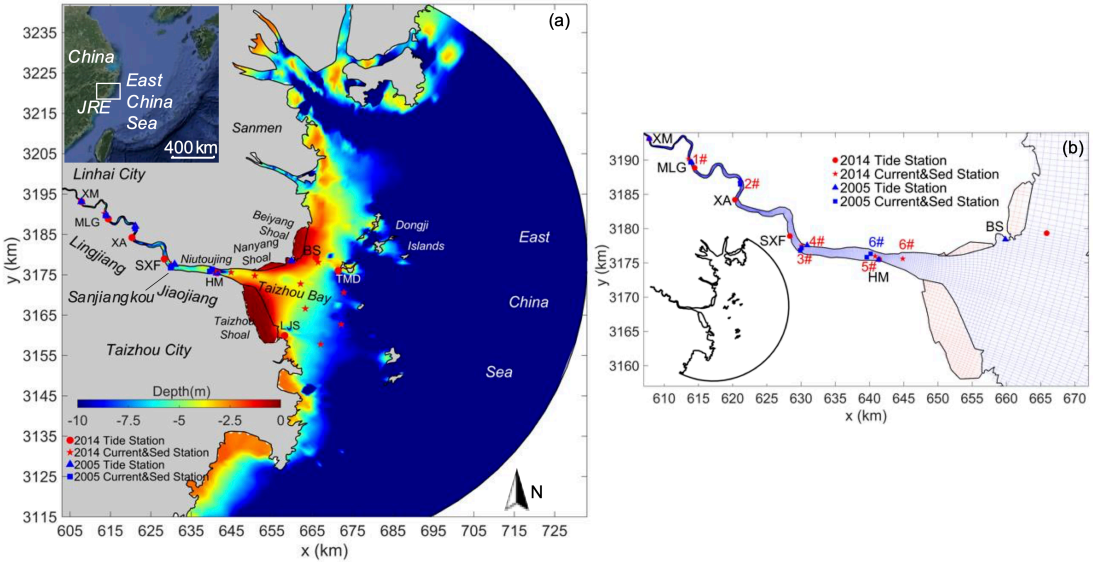

Figure 1. Location and bathymetry of the Jiaojiang River Estuary (a); model grids, red lines are used for reclamation area in from 2005 to 2014 (b).

DATA AND METHODS

Study area and data

The JRE, located in central Zhejiang Province, China, consists of three sections: the Lingjiang River, the Jiaojiang River, and the JRE. The Lingjiang River flows through Linhai City and is referred to as the Jiaojiang River after reaching Sanjiangkou downstream of Shixianfu (SXF). It then flows into Taizhou Bay through Niutoujing (the river mouth), beyond which lies the JRE and Taizhou Bay (see Fig. 1a). The JRE exhibits strong tidal characteristics, with an average tidal range of approximately 4.0 m and a maximum of 6.3 m. The average durations for flood and ebbing tides are 5.1 hours and 7.3 hours, respectively. The suspended sediment in the JRE primarily consists of silt and clay, with majority originating from marine sources and the median grain size ranges between 4 to 9 μm.

According to relevant studies, from 1983 to 2004, evacuating sand in the Lingjiang River and Jiaojiang River channels extracted over 40 million m^3, reducing the average riverbed elevation by 1.98 m (Chen et al., 2008). From 1984 to 2013, the coastline on both the northern and southern sides of the JRE extended seaward (Zhang et al., 2016). The Taizhou Shoal on the southern side advanced at an average rate of 5,000 m per year, and the Nanyang and Beiyang shoals on the northern side advanced at rates of 67 and 110 m per year, respectively, resulting in about 106 km^2 of reclaimed tidal flats. Subsequent to extensive human activities, the hydrodynamics and morphology of the JRE have rapidly evolved.

This study involved two hydro and sediment surveys and the collection of topographic data in September 2005 and June 2014. In 2005, the survey deployed 6 fixed current and sediment stations and 6 tide stations in the river channel. In 2014, the survey expanded to include 5 current and sediment stations (1#~5#) and 6 tide stations in the river channel, as well as 8 additional current and sediment stations (6#~13#) in the offshore area. These data were utilized for analysis, model calibration and validation. The study area and station layout are depicted in Figure 1a, using the CGCS2000 (Chinese Geodetic Coordinate System 2000).

3-D Numerical Model

The Delft3D software (Deltares, 2024) was utilized to develop a three-dimensional hydro, sediment and salt model for the JRE, employing orthogonal curvilinear and σ-coordinate system for the model's horizontal and vertical orientations. The governing equations for three-dimensional flow, sediment and salinity transport in the model are based on the N-S equations and the sediment and salinity convection-diffusion equation, respectively.

The model's computational area encompasses the Lingjiang River section, the Jiaojiang river section, and the Taizhou Bay. The upstream boundary is positioned at 6 km upstream of the Ximen (XM), while the sea boundary extends 70 km seaward in an arc centered on the estuary's mouth. The model's horizontal grid resolution is 739 × 616 (Fig. 1b), featuring finer grid spacing of approximately 25 m

across the river's width and 70 m along its length in the upstream region. Vertically, the grid is divided into 10 layers.

Model topography was derived by interpolating topographic data measured in 2005 and 2014. To facilitate comparative analysis of the reclamation's impact on the estuarine hydro and sediment dynamics, these two models shared identical parameters (see in Table 1), differing only in topography and morphology. The upstream flow boundary was set based on 2014 flood season discharge data, and the sea boundary was defined using astronomical tidal constituent parameters from TPXO. The upstream salinity boundary was 0, while the downstream was 28-30‰. Sediment inputs at the boundaries were excluded to stress the analysis of sediment erosion in the channel and internal sediment sources.

The model underwent validation by assessing tide levels, currents, and SSC during the spring tide of September 2005 and June 2014, with partial results presented in Figure 2. Statistically, the correlation coefficients for tide levels, current magnitude, directions, and SSC between measured and simulated values were 0.921, 0.780, 0.852 and 0.536 in 2005 and 0.988, 0.815, 0.865, and 0.642 in 2014, respectively. These values demonstrate the model's strong capability to accurately simulate both the dynamic processes and sediment transport in the JRE.

Table 1. Specification of some model parameters

Parameter	Description	Value
n	Bottom roughness	0.013~0.025 s/m$^{1/3}$
υ_H	Background horizontal eddy viscosity	1 m^2/s
D_H	Background horizontal eddy diffusivity	1~150 m^2/s
γ_s	Sediment specific density	2650 kg/m^3
γ_0	Sediment dry bed density	735 kg/m^3
w	Settling velocity	0.5 mm/s
M	Erosion parameter	0.0035 kg/m^2/s
$\tau_{cr,d}$	Critical bed shear stress for sedimentation	1000 N/m^2
$\tau_{cr,e}$	Critical bed shear stress for erosion	0.4 N/m^2

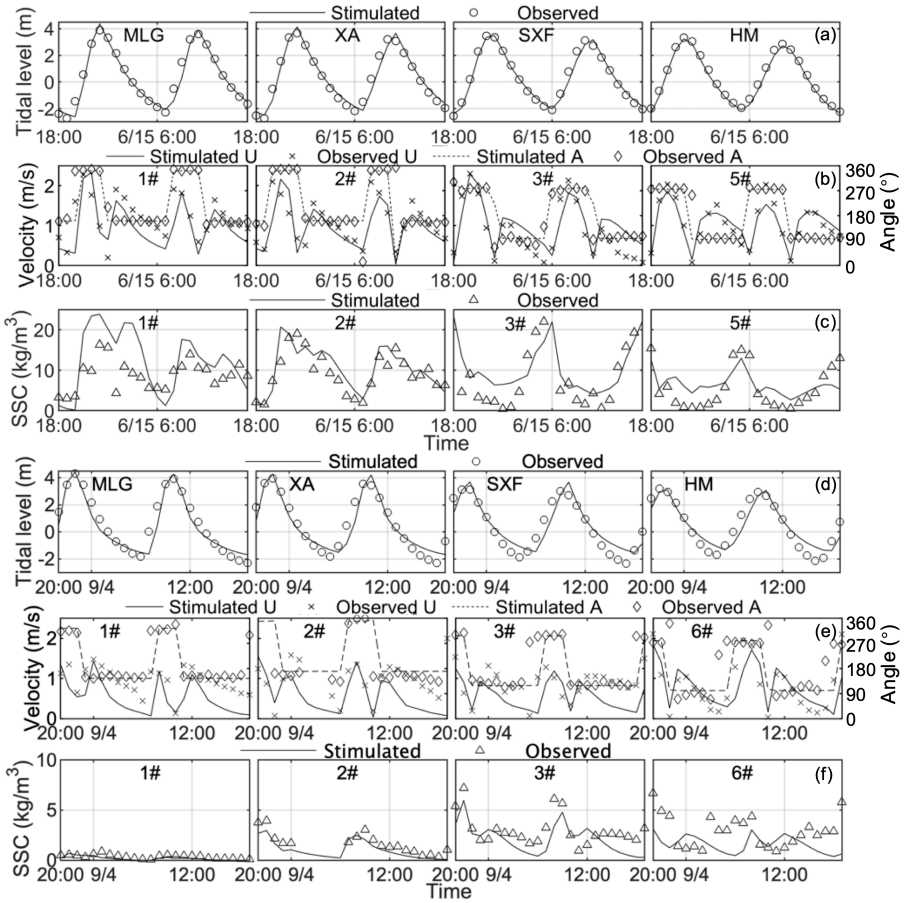

Figure 2. Validation on model results in 2014 for tidal level (a), current velocity and angle (b) and SSC (c). The same applies for 2005 (d ~ f).

Mechanism decomposition of sediment flux

To investigate the causes of sediment transport variations in the JRE, sediment flux at each current and sediment station was decomposed using the mechanism decomposition of sediment flux method (Dyer, 1974):

$$T_S = \frac{1}{T}\int_0^T \int_0^h ucdz\,dt$$

$$= \underbrace{h_0\bar{u}_0\bar{c}_0}_{T_1} + \underbrace{\langle h_t\bar{u}_t\rangle\bar{c}_0}_{T_2} + \underbrace{\langle h_t\bar{c}_t\rangle\bar{u}_0}_{T_3} + \underbrace{h_0\langle\bar{u}_t\bar{c}_t\rangle}_{T_4} + \underbrace{\langle h_t\bar{u}_t\bar{c}_t\rangle}_{T_5} + \underbrace{h_0\langle\overline{u'c'}\rangle}_{T_6} + \underbrace{\langle h_t\overline{u'c'}\rangle}_{T_7} \quad (1)$$

Where: T_S represents the total transport, with $\langle\ \rangle$ indicating tidal cycle averaging and the overline signifying vertical averaging. The seven terms on the right-side detail various transport mechanisms: T_1 involves sediment transport by Eulerian residual velocity (ERV). T_2 pertains to tides and tidal currents (i.e., Stokes drift sediment transport). T_3~T_5 relate to tidal changes in sediment concentration due to tide, currents and tide together with currents; T_6 denotes sediment transport by vertical gravitational circulation; T_7 covers changes in current velocity and sediment concentration caused by tidal wave deformation. The groups $T_1 + T_2$, $T_3 + T_4 + T_5$ and $T_6 + T_7$ correspond to Lagrangian advection transport, tidal pumping transport, and vertical net circulation transport, respectively.

RESULTS

Results of observed data

Hydrodynamic. The measured tide level from the JRE during the flood seasons of 2005 and 2014 are depicted in Figures 3a and 3b, showing maximum tide levels, tidal ranges, and durations of flood and ebbing tides. The figures indicate minimal changes in maximum tide levels outside the JRE from 2005 to 2014, with a slight increase between SXF and Haimen (HM), and a decrease from SXF towards upstream. Significant changes occurred in the tidal range of the JRE; in 2005, the maximum tidal range increased from the mouth towards upstream (a peak of 6.7 m at Miaolonggang, MLG) before decreasing further towards upstream. In 2014, it kept increasing up to 6.85 m at XM. Besides, significant changes were also observed at the same stations. For example, the maximum tidal range at the Baisha (BS) station outside the mouth increased by approximately 0.5 m, and subsequently decreased by the same amount at MLG, before increasing again towards upstream to 0.6 m. Tidal asymmetry in the JRE is pronounced. At BS, the difference between flooding and ebbing tides remains small, with flooding tides shortening and ebbing tides lengthening towards upstream. For instance, at the HM station, flooding tide duration increased by 0.1 h, and at the XM station, by about 0.5 h, with corresponding decreases in ebbing tide durations.

Accurate analysis of the tidal structure is essential for precisely describing sediment transport. Figure 3c displays the vertical residual current distribution during flood season spring tides for each testing line (1#~6#) in the JRE, with positive values indicating seaward currents and negative values indicating landward. According to Figure 3c, in the upstream Lingjiang River section (1# and 2#), the Lagrangian residual velocity (LRV) decreased by approximately 0.1 m/s in 2014 compared to 2005, with the current at the bottom of 2# even reversing to flow upstream. 3# and 4# are situated in the downstream bend of the SXF, with 3# on the southern bank. Here, the LRV at the middle and bottom layers increased by approximately 0.1 m/s after reclamation, while the surface layer and the southern bank still experienced a decrease. 5# in 2014 and 6# in 2005 are located at similar positions where the depth is greatest at Niutoujing. After reclamation, both the LRV and ERV reversed upstream, with a dominant flooding current and high velocity. The 6# in 2014 was located upstream of the reclamation area. Here, the residual current values were significantly reduced compared to upstream, with velocity remaining below 0.2 m/s, while near upstream of Niutoujing, the velocity could reach up to 0.43 m/s.

Sediment dynamics. Figure 3d illustrates the SSC time series at each testing line. In 2005, the maximum SSC at 1# and 2# were less than 3 kg/m^3, whereas concentrations at the bottom of other lines reached up to 12 kg/m^3 or 15 kg/m^3. At the onset of flooding tide, sediments accumulate at 5# and 6#. By flooding tide's end, SSC at 3# decreases, while at 2#, it remains relatively unchanged, suggesting sediment migration occurs between 2# and 3#. After ebbing tide, high concentrations at 4# and 5# reappeared, while the 6# in 2005 (HM) did not show a significant increase, suggesting the sediment mobilized during the flooding tide had been deposited in the upstream river channel during the ebbing tide.

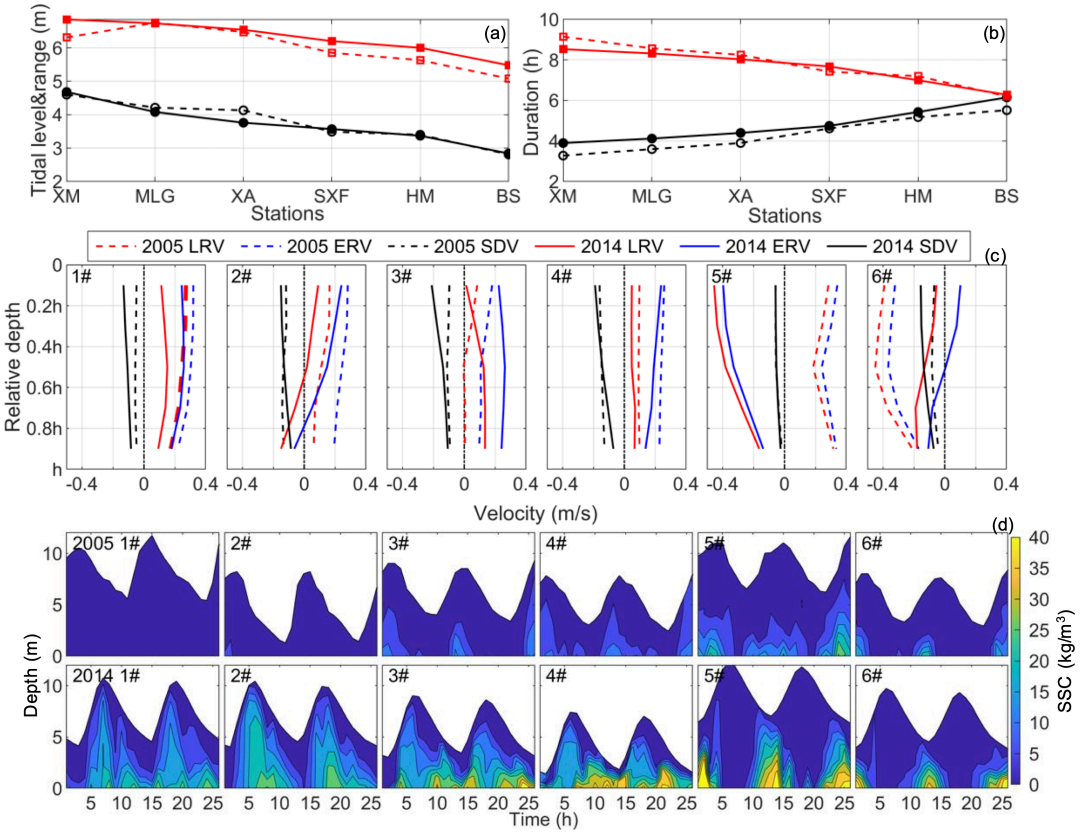

Figure 3. Observed results of flow and SSC in the JRE in 2005 and 2014 (dashed lines represent 2005, solid lines represent 2014): maximum high tide level and maximum tidal range, with the black line indicating tidal level and the red line indicating tidal range (a); flood and ebb durations, with the black line representing flood duration and the red line representing ebb duration (b); vertical residual flow distribution (c), positive values indicate the seaward direction, and negative values indicate the landward direction; and SSC distribution (d).

After reclamation, SSC in the JRE surged, peaking at 39 kg/m^3 at 3# to 6# in 2014 (triple the pre-reclamation). SSC at the bottom of 1# and 2# reached 24 kg/m^3, signifying a substantial increase in total amount of sediment and a dramatic expansion in the range of sediment movement towards upstream. Sediment movement in the JRE extended upstream to the 1# from within the original Jiaojinag River after reclamation. Additionally, at the end of ebbing tide in 2014, SSC at 5# (HM) began to increase, suggesting sediment replenishment from upstream.

Results of numerical model

Tidal wave variation. Based on results of the model, harmonic analysis was conducted on the tide levels (Pawlowicz et al. 2002), with six tidal constituents of larger amplitudes selected for display in Figure 4a and 4b. The figure reveals that the M2 constituent is dominant in JRE. After reclamation, the M2 amplitude increased towards upstream in the river (0.3 m at HM and approximately 0.8 m at XM). Conversely, M4 amplitude decreased by about 0.1 m from the Xiao (XA) to HM, with minimal changes upstream. These changes resulted in a decrease in the ratio of the M4 to the M2 amplitude by 0.06~0.11 after reclamation (Fig. 4c), but both these ratios increased towards upstream. The phase difference between M2 and M4 increased by 3 to 16 degrees from 2005 to 2014, and all increased from mouth towards upstream. The difference remained between 30° and 60° before and after the reclamation, with flooding tides still dominating.

Shift of the ETM. Figure 4d displays the distribution profile of tidal average SSC along the centerline. As shown in the figure, the Lingjiang River section experienced the greatest siltation from 2005 to 2014, with most of the riverbed accumulating nearly 2 m, while the area outside HM was an erosion zone. In 2005, from SXF to HM housed the primary turbidity zone, with SSC averaging 6 kg/m^3 or less. By 2014, SSC in this section had nearly doubled to 10 kg/m^3. The range of SSC exceeding 10 kg/m^3 extended 21 km from XM to SXF, where even surface SSC reached 5 kg/m^3. Statistically, from

2005 to 2014, the tidal average SSC from XM to SXF rose by 5 kg/m^3, from SXF to HM by 3 kg/m^3, while outside HM, it remained relatively unchanged.

Figures 4e and 4f illustrate the movement of the ETM at different times. During flooding tide, SSC in the bottom layer of ETM was within 15 kg/m^3 in 2005, increasing to 30 kg/m^3 in 2014 (an increase of approximately 15 kg/m^3). Using 10 kg/m^3 as the threshold for SSC, the ETM extended up to 57 km upstream from the mouth (between SXF and XA) in 2005, with a maximum length of 16 km at the start of ebbing tide. In 2014, the ETM extended to the upper reach near XM, 90 km from the mouth, with a length of up to 43 km. This indicates a significant expansion in both the distribution and movement ranges of the ETM after the reclamation. Furthermore, the duration of the ETM also increased. In 2005, it was most pronounced at the end of flooding tide and the beginning of ebbing tide, with SSC dropping below 10 kg/m^3 by ebbing tide. In contrast, by 2014, SSC exceeded 10 kg/m^3 in an 8 km river section even at the end of ebbing tide.

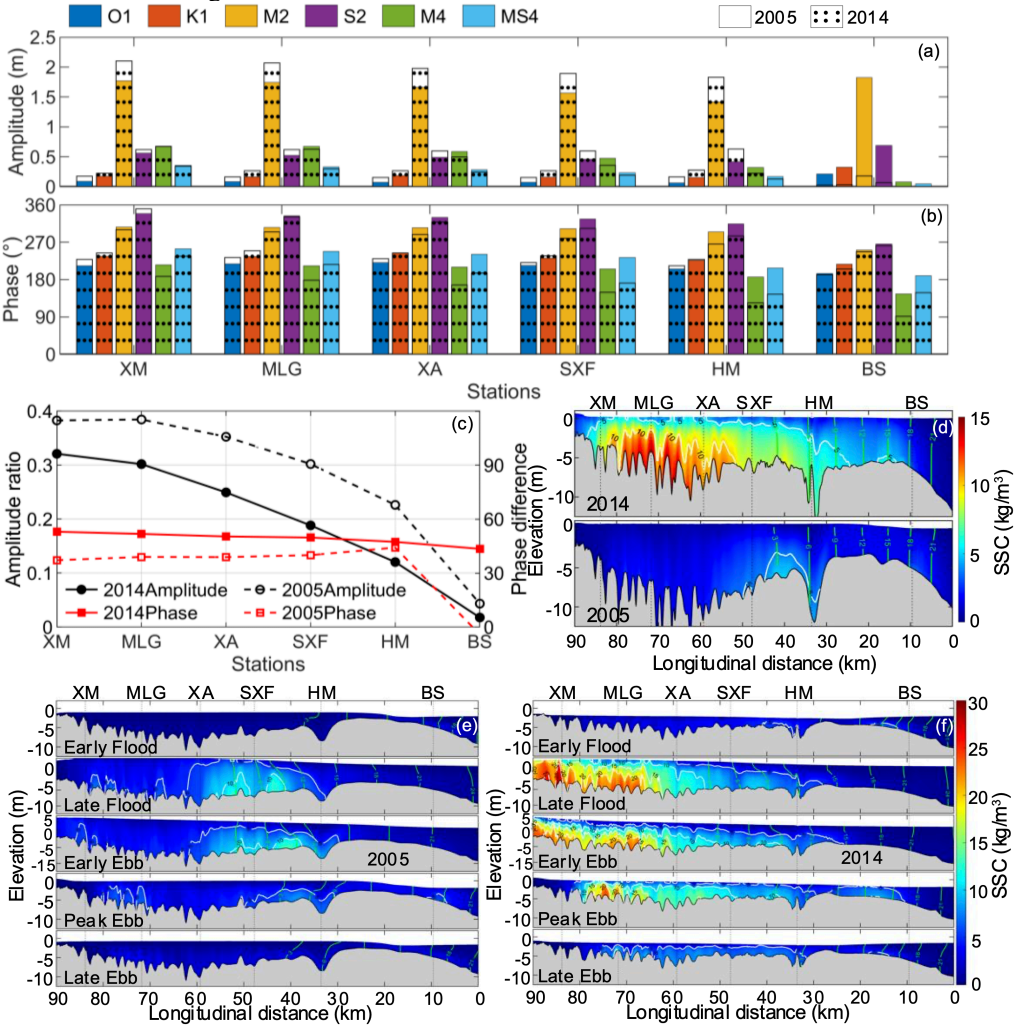

Figure 4. Results of hydrodynamic and sediment transport model for the JRE in 2005 and 2014: amplitudes (a) and phases (b) of part tide constituents, with solid colors representing 2005 and dotted patterns representing 2014, specific constituent names are shown in the top left corner of the figure; amplitude ratio (A_{M4}/A_{M2}, black line) and phase difference ($2g_{M2}-g_{M4}$, red line), with solid lines for 2014 and dashed lines for 2005 (c); tidal average SSC distribution with white contour lines for SSC and green contour lines for salinity (d); ETM movement processes in 2005 (e) and 2014 (f).

DISCUSSION

Impact of reclamation on hydrodynamics

The reclamation significantly altered the morphology of the JRE, narrowing the originally open 'trumpet mouth'. The tidal wave energy becomes more concentrated in this area, resulting in a significant

increase in the M2 amplitude. As tidal waves propagate shoreward, increased water depth at the mouth reduces the deformation of shallow water constituents. This results in decreased tidal asymmetry and prolonged flooding tide durations. Despite these changes, the amplitude of the M2 and the overall tidal range have both increased after the reclamation.

Initially, following the reclamation and before significant topographic changes, the narrowing of the mouth increased the current velocity into the estuary and simultaneously boosted the unit width discharge, resulting in higher tidal levels. The increased velocity raised bottom shear stress outside HM, mobilizing more bed sands into the water column. This led to scouring near the mouth, decreasing the bed elevation and altering the actual topography. The reduction in bed elevation has led to an increase in water depth in this section. Comparing the results of the two hydrological surveys, the water depth in the area has increased, and the bed roughness has decreased, further increasing the current velocity. The vertical distribution curve of LRV shifted leftward (Fig. 3c), indicating a strengthening of flooding currents, even as the duration of flooding tide increased post-reclamation. From XM to HM, the vertical LRV distribution curves similarly shift to the left, with flooding tides being strengthened, causing the water to move further upstream. In the JRE, flooding tides dominate. After the reclamation, sediment outside HM is transported upstream by the flooding tide and settles during the ebbing tide, leading to sediment accumulation from XM to HM. This causes the bed slope along the river to decrease, resulting in a gentler topography, which makes it easier for the flooding tide water outside HM to be transported further upstream.

Impact of reclamation on sediment dynamics

Tidal and current asymmetry is the primary driver of ETM formation and sediment transport in the JRE. It also serves as the main mechanism through which the reclamation impacts ETM movement. During flooding tides, once the critical shear stress is reached, sediment begins to mobilize, entering the water column and being transported upstream by the flow. Simultaneously, sediment from upstream regions also mobilizes, resulting in high SSC within a specific area, which leads to the formation and upstream expansion of the ETM. After the peak flooding tide, as velocity decreases, the amount of mobilized sediment becomes less than that settling, causing an overall reduction in SSC. This trend starts from the downstream area, and the ETM appears to shift towards upstream. Sediment deposition lags behind the tidal current, allowing the ETM to persist until the ebbing tide. During the ebbing tide, it gradually shifts downstream, with SSC decreasing after the peak ebbing tide.

The reclamation in the JRE has increased the flood current velocity, leading to higher shear stress between the water column and the riverbed. This increased shear stress mobilizes more sediment, allowing it to reach higher layers in the water column, even up to the surface (Fig. 3d), thereby increasing the SSC in the area. Additionally, the increased velocity in the upper water layers facilitates the transport of sediment towards the upper layers of the upstream water column following the reclamation. Sediment remains suspended in the water column for a longer duration, with increased settling time, allowing it to travel further upstream and at a faster pace. Therefore, during flooding tides, the SSC in the ETM becomes higher, the sediment moves further upstream, at a faster speed, and persists for a longer duration.

In 2005, the core SSC in the ETM was only 10 kg/m^3. Sediment began settling to the bed by the end of flooding tide, restricting the movement of the ETM from SXF to HM without extending further upstream. In contrast, by 2014, the SSC at the core of the ETM had increased to over 30 kg/m^3. The delayed settling of sediment persisted until the ebbing tide, with sediment being transported downstream during the ebb. Throughout this downstream movement, the overall trend was one of gradual sediment settling, but even by the end of the ebbing tide, 5 kg/m^3 of sediment remained suspended in the water column, lingering into the early part of the next tidal cycle. Additionally, the reclamation led to an increase in the duration of the flooding tide, amplifying the dominance of the flood current. The prolonged flooding tide allowed sediment to remain suspended in the water column more easily, extending the time during which sediment could be mobilized and reducing the time available for sediment to settle.

Impact of reclamation on sediment transport mechanisms

According to the mechanism decomposition of sediment flux shown in Figure 5, vertical net circulation contributes minimally, so the focus in the following analysis is on advective transport and tidal pumping transport. In the JRE, sediment transport is primarily dominated by tidal pumping effect, with advective transport playing a secondary role. For advective transport, ERV transports sediment (T_1) downstream across the entire river, while Stokes drift transports sediment (T_2) upstream. In 2014, the increase in sediment transport flux due to ERV from XM to HM exceeded that of Stokes drift sediment

transport, indicating that the reclamation has led to an enhanced capacity for downstream sediment transport via advection in the JRE. This increasing trend extends up to 9 km outside HM, near the outer boundary of the reclamation area.

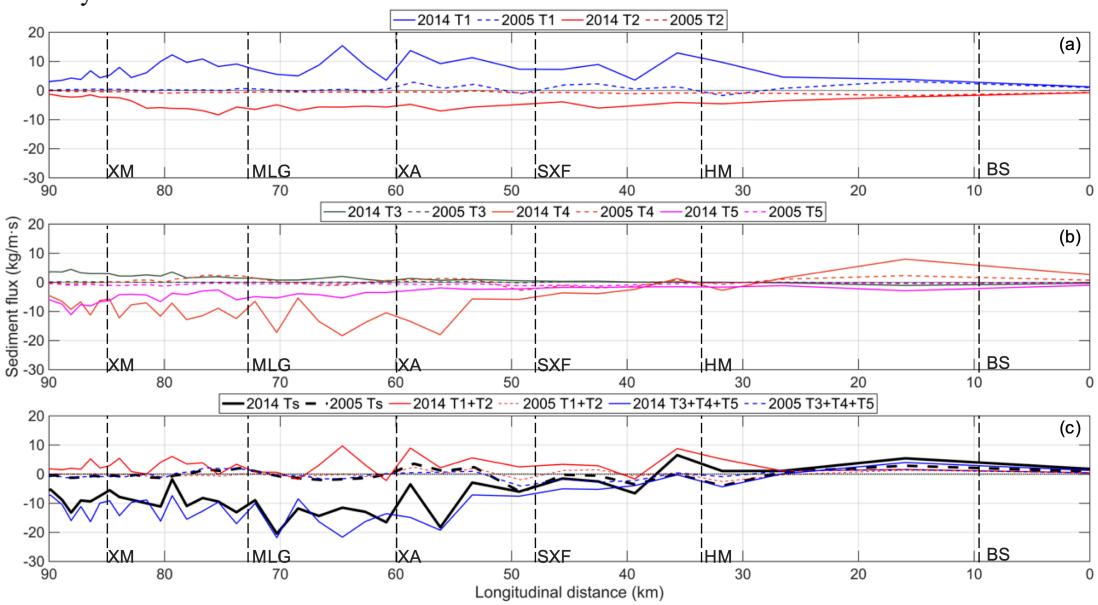

Figure 5. Mechanism decomposition of suspended sediment flux (solid lines represent 2014, dashed lines represent 2005, and specific colors are shown in each legend, positive values indicate seaward transport, while negative values indicate landward transport): advective sediment transport T1~T2 (a); tidal pumping sediment transport T3~T5 (b); and total sediment transport Ts (c).

Conversely, the increase in tidal pumping effects following the reclamation is more pronounced than that of advective transport. Among the three components of tidal pumping, only the component related to the interaction between tides and SSC variations (T_3) directed seaward, showing a slight increase compared to before the reclamation, but its magnitude is very small, contributing little to the overall tidal pumping effect. The main contributors are the components related to the interaction between currents and SSC variations (T_4), as well as the interaction among tides, currents, and SSC variations (T_5). These two components consistently point landward from XM to SXF. Before the reclamation, their magnitudes were small, but after the reclamation, they increased significantly. The T_4 is generally larger than T_5 across most sections of the river. This trend continues until SXF, where it gradually weakens, eventually resulting in seaward fluxes. The magnitude of these fluxes becomes similar to the pre-reclamation levels, and near HM, they shift back to a landward direction, continuing to increase as they come outside HM. Overall, the tidal pumping effect demonstrates that sediment is transported upstream from XM to SXF, but the effect weakens as it enters the section downstream the SXF. However, in both directions, the sediment transport fluxes have significantly increased throughout the entire river section.

It is evident that from XM to SXF, tidal pumping consistently dominates, with a direction pointing upstream. The increase in this component is the primary reason for the significant upstream movement of sediment in this section. From SXF to HM, the influence of tidal pumping decreases as it moves downstream, gradually being overtaken by positive advective transport. The transport direction shifts from upstream transport near SXF to downstream transport near HM. The increase in advective sediment transport flux leads to enhanced downstream sediment transport. In the area outside HM, the various processes interact and combine, resulting in net sediment transport downstream. Although the magnitude of sediment transport in this section is smaller compared to upstream sections, it has still increased compared to pre-reclamation levels.

This change in sediment transport characteristics causes sediment downstream of HM to be transported laterally. Upstream-transported sediment moves further upstream during flooding tides and begins to settle at the start of the ebbing tide. A significant amount of sediment completes the settling process before reaching the SXF, leading to siltation from XM to SXF. The remaining sediment in the water column continues to move downstream with the ebbing tide, completing the settling process from SXF to HM, resulting in slight siltation in that section. Outside HM, sediment is primarily transported upstream, becoming the main source of sediment for the JRE and causing erosion in this area.

CONCLUSIONS

Our study, combining data analysis with a hydro and sediment dynamics numerical model, examines the transitions in tidal dynamics, sediment dynamics, and the behavior of the ETM in the JRE before and after the reclamation. The main conclusions are as follows:

1. After the reclamation, tidal level adjustments were not significant, but the tidal range increased notably. The M2 amplitude increased, and tidal asymmetry weakened, although flooding tides still predominated. The flood current velocity increased, and the LRV in the river upstream the HM continued to point downstream, with a decrease in velocity. Downstream the HM, the flow direction shifted upstream, with little adjustments in velocity.
2. After the reclamation, the maximum SSC at the bottom of the JRE increased from 12 kg/m^3 to 39 kg/m^3. The tidal average SSC in the Lingjiang River increased by 5 kg/m^3, while that in the Jiaojiang River from SXF to the HM increased by 3 kg/m^3. The distribution and movement range of the ETM expanded by nearly 30 km, leading to significant siltation from XM to SXF, while areas downstream HM experienced erosion.
3. Tidal asymmetry is the primary cause of the formation of the ETM in the JRE, where sediment transport is predominantly driven by tidal pumping, with advection playing a secondary role. After the reclamation, the significant intensification of tidal pumping in the river sections near and above SXF led to a substantial upstream transport of sediment. This is the main reason for the increased SSC, the upstream shift of the ETM, and transitions in its duration.

REFERENCES

Burchard, H., Schuttelaars, H. M. and Ralston, D. K., 2018. Sediment trapping in estuaries. *Annual Review of Marine Science*, 10(1): 371-395.

Chen, F. Y., Hu, J. C., Bai, X. Y., Huang, S. C. and Gao, H. C., 2008. Effect of evacuating sand on Jiaojiang River estuary. *Journal of Sediment Ressearch*, 33(3): 46-53.(in Chinese)

Dai, Z., Liu, J. T., Wei, W. and Chen, J., 2014. Detection of the three gorges dam influence on the Changjiang (Yangtze River) submerged delta. *Scientific Reports*, 4(1): 6600.

de Jonge, V. N., Schuttelaars, H. M., van Beusekom, J. E. E., Talke, S. A. and de Swart, H. E., 2014. The influence of channel deepening on estuarine turbidity levels and dynamics, as exemplified by the Ems estuary. *Estuarine, Coastal and Shelf Science*, 139: 46-59.

Deltares, 2024. Delft3D-Hydro-Morphodynamics User Manual.

de Swart, H. E., Schuttelaars, H. M. and Takle, S. A., 2009. Initial growth of phytoplankton in turbid estuaries: A simple model. *Continental Shelf Research*, 29(1): 136-147.

Dyer, K. R., 1974. The salt balance in stratified estuaries. *Estuarine and Coastal Marine Science*, 2(3): 273-281.

Glangeaud, L., 1938. Transport et sédimentation dans l'estuaire et à l'embouchure de La Gironde. *Bulletin de la Société géologique de France*, 5e série, 8: 599-631.

Guan, W., Wolanski, E. and Dong, L., 1998. Cohesive sediment transport in the Jiaojiang River Estuary, China. *Estuarine, Coastal and Shelf Science*, 46(6): 861-867.

Jay, D. A., Talke, S. A., Hudson, A. and Twardowski, M., 2015. Estuarine turbidity maxima revisited: Instrumental approaches, remote sensing, modeling studies, and new directions. *Developments in Sedimentology*, 68: 49-109.

Mitchell, S., Akesson, L. and Uncles, R., 2012. Observations of turbidity in the Thames Estuary, United Kingdom. *Water and Environment Journal*, 26(4): 511-520.

Pawlowicz, R., Beardsley, B. and Lentz, S., 2002. Classical tidal harmonic analysis including error estimates in MATLAB using T_TIDE. *Computers and Geosciences*, 28(8): 929-937.

Sun, Z., Huang, S., Jiao, J., Nie, H. and Lu, M., 2017. Effects of cluster land reclamations on storm surge in Jiaojiang Estuary, China. *Water Science and Engineering*, 10(1): 59-69.

Tessler, Z. D., Vörösmarty, C. J., Grossberg, M., Gladkova, I., Aizenman, H., Syvitski, J. P. M. and Foufoula-Georgiou, E., 2015. *Profiling risk and sustainability in coastal deltas of the world. Science*, 349(6248): 638-643.

Wang, W., Liu, H., Li, Y. and Su, J., 2014. Development and management of land reclamation in China. *Ocean and Coastal Management*, 102: 415-425.

Winterwerp, J. C., 2011. Fine sediment transport by tidal asymmetry in the high-concentrated Ems River: indications for a regime shift in response to channel deepening. *Ocean Dynamics*, 61(2-3):203-215.

Yao, Y., Chen, X., Yuan, J., Li, L. and Guan, W., 2023. Impacts of channel dredging on hydrodynamics and sediment dynamics in the main channels of the Jiaojiang River Estuary in China. *Acta Oceanologica Sinica*, 42(9): 132-144.

Yu, Y., Zhang, H. and Lemckert, C., 2014. Salinity and turbidity distributions in the Brisbane River estuary, Australia. *Journal of Hydrology*, 519: 3338-3352.

Zhang, Q., Fan, D., Tao, J., Tu, J. and Guo, X., 2022. Impacts of land reclamations on hydrodynamics and morphodynamics in the highly altered North Branch of the Changjiang Estuary. *Anthropocene Coasts*, 5: 6.

Zhang, Q., Tao, J. and Yang, J., 2016. Numerical study on the transport timescale in a river-influenced macro-tidal estuary. *Journal of Coastal Research*, 75(sp1): 193-197.